International Journal of Nanomedicine

Dovepress
open access to scientific and medical research

Open Access Full Text Article

ORIGINAL RESEARCH

Gadolinium Oxide Nanoparticles Reinforce the Fractionated Radiotherapy-Induced Immune Response in Tri-Negative Breast Cancer via cGAS-STING Pathway

Boyi Yu[1–4], Xuanyi Lu[5], Xianglong Feng[1–4], Ting Zhao[1–4], Jiaxin Li[1–4], Yudie Lu[5], Fei Ye[1–4], Xiongxiong Liu[1–4], Xiaogang Zheng[1–4], Zheyu Shen[5], Xiaodong Jin[1–4], Weiqiang Chen[1–4], Qiang Li[1–4]

[1]Biomedical Center, Institute of Modern Physics, Chinese Academy of Sciences, Lanzhou, People's Republic of China; [2]Key Laboratory of Heavy Ion Radiation Biology and Medicine, Chinese Academy of Sciences, Lanzhou, People's Republic of China; [3]Key Laboratory of Basic Research on Heavy Ion Radiation Application in Medicine, Lanzhou, Gansu Province, People's Republic of China; [4]College of Life Sciences, University of Chinese Academy of Sciences, Beijing, People's Republic of China; [5]School of Biomedical Engineering, Southern Medical University, Guangzhou, People's Republic of China

Correspondence: Xiaodong Jin; Weiqiang Chen, Institute of Modern Physics, Chinese Academy of Sciences, 509 Nanchang Road, Lanzhou, Gansu Province, 730000, People's Republic of China, Tel +86-931-4969316, Fax +86-931-8272100, Email jinxd@impcas.ac.cn; chenwq7315@impcas.ac.cn

Introduction: Radiotherapy is a widely recognized first-line clinical treatment for cancer, but its efficacy may be impeded by the radioresistance of advanced tumors. It is urgent to improve the sensitivity of radioresistant tumors to radiotherapy. In this work, gadolinium oxide nanocrystals (GONs) were utilized as radiosensitizers to enhance the killing effect and reinforce the immune activation of X-ray irradiation on 4T1 breast cancer cells in vitro and in vivo.

Methods: 1.0 T small animal MR imaging (MRI) system was employed to trace GONs in vivo, while 225 kVp X-ray irradiation equipment was utilized for investigating the radiosensitization of GONs in 4T1 breast cancer cells in vitro and in vivo. Western blot, quantitative real-time PCR (RT-qPCR), immunohistochemistry, immunofluorescence, clonal survival assay, flow cytometry and reactive oxygen species assay were used to explore the biological mechanism of GON sensitization.

Results: GONs exhibited exceptional utility as contrast agents for both in vivo and in vitro MRI imaging. Interestingly, a single dose of 8.0 Gy X-rays together with GONs failed to confer superior therapeutic effects in tumor-bearing mice, while only 3.0 Gy × 3 fractions X-rays combined with GONs exhibited effective tumor growth inhibition. Moreover, fractionated X-ray irradiation with GONs demonstrated a superior capacity to activate the cGAS-STING pathway.

Discussion: Fractionated X-ray irradiation in the presence of GONs has demonstrated the most significant activation of the anti-tumor immune response by boosting the cGAS-STING pathway.

Keywords: gadolinium oxide nanoparticles, magnetic resonance imaging, radiosensitization, cGAS-STING pathway, 4T1 breast cancer cells

Introduction

According to the World Health Organization, there were about 19.3 million new cancer cases worldwide in 2020. Breast cancer ranks the first in incidence and fourth in mortality among female patients, which greatly threatens the health of women.[1] Radiation therapy is one of the most important modalities in the clinical breast cancer treatment as well as surgery and chemotherapy.[2] More than half of the patients need radiation therapy.[3] Although radiotherapy serves as a frontline treatment for more than half of the patients with malignancies, its therapeutic effect is still limited by tumor hypoxia, tumor immune evasion, and tumor radioresistance.[4] Therefore, how to develop theranostic agents to improve the sensitivity of radioresistant tumors to radiotherapy is one of the problems to be solved urgently in clinical treatment of tumors.[5,6] In recent years, high-Z metal nanoparticles have emerged as a promising class of tumor radiosensitizers.[7,8]

Received: 20 August 2023
Accepted: 2 December 2023
Published: 15 December 2023

Graphical Abstract

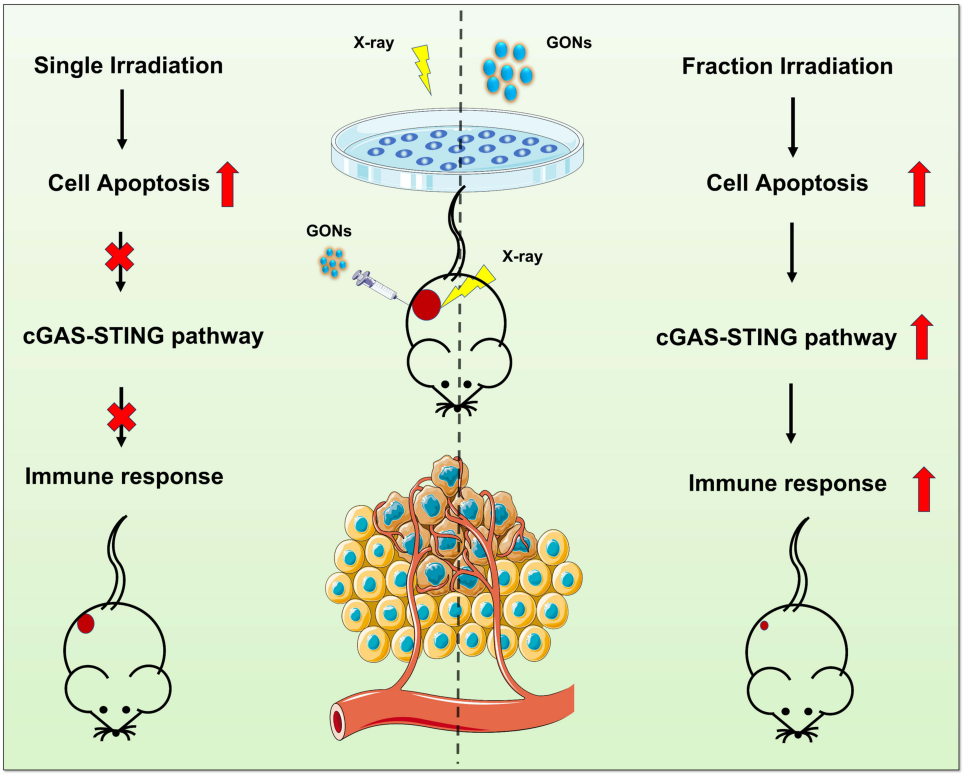

These materials possess a high X-ray photon capture cross-section, which intensifies the production of secondary and Auger electrons, leading to an increment in reactive oxygen species (ROS) productivity and ultimately enhancing the efficacy of radiotherapy.[9,10] Moreover, the use of targeting biomolecules or enhanced permeability and retention (EPR) effect allows nanomaterials containing high-Z atoms to accumulate and concentrate selectively in tumors, providing an opportunity for their development as nano-enhancers that improve the biological effect of irradiated physical dose.[11] Gold nanoparticles have demonstrated radio-enhancement effects both in vitro and in vivo and can be applied as theranostic agents in computed tomography-guided radiotherapy.[7,8,12,13]

Magnetic resonance imaging (MRI)-guided radiotherapy represents a state-of-the-art image-guided radiotherapy (IGRT) technique, providing an effective imaging modality for soft tissue as an alternative approach.[14] Gadolinium-based compounds have garnered widespread use as contrast agents in clinical MRI owing to their demonstrated efficacy in augmenting the signal-to-noise ratio between tumorous and normal tissues.[15] In recent years, gadolinium-based nanoparticles (GdNPs), with their high atomic number (Z = 64) and long relaxation time, have emerged as promising theranostic agents.[16–24] Furthermore, ultrasmall gadolinium oxide nanocrystals have been demonstrated to be an advanced T1-weighted MRI contrast agent, characterized by high longitudinal relaxation and small r_2/r_1 ratios.[25–27] Significantly, the Gd content of this contrast agent is notably high, at approximately 200–400 Gd ions per particle.[28] In the previous study, we found that the presence of GONs enhanced the apoptosis and autophagy of lung cancer cells induced by ionization radiation in vitro.[29,30] MRI provides superior soft tissue resolution compared to CT scanning, due to its ability to combine anatomical and functional imaging. Notably, GONs serve as both radiosensitizers and contrast agents for MRI, making the use of GONs an optimal choice for IGRT.[31] Another merit making MRI a better candidate for IGRT is that no additional dose produced in patients by the equipment, which is desirable when considering the "as low as reasonably achievable" (ALARA) principle.[32] Amirrashedi and coworkers investigated the radiosensitization property of GdNPs, the maximum dose enhancement of GdNPs ranged in 15%~24%.[33] Seo and coworkers found that the

enhancement of GdNPs was dose-dependent with a maximum factor 1.94 in the production of ROS under photon and proton irradiation compared with the radiation-only control.[34] Shen et al developed novel GONs with high biocompatibility which enhanced the radiation therapy of GBM as an effective radiosensitizing agent.[35] Song et al showed that gadolinium-based nanoparticles AGuIX combined with low-dose irradiation can better activate anti-tumor immune response in vivo, and also enhance the efficacy of PD-L1 antibody.[36] In the study by Zhang et al, it was found that AGuIX was capable of enhancing macrophage polarization from M2 to M1.[37] Sun et al showed that AGuIX can enhance inhibition of triple negative breast by modulating the NRF2-GSH-GPX4 signaling pathway.[22]

It is well known that the generation of ROS is able to attract and activate effector cells of the innate immune system which are triggered to mount phagocytic and cytotoxic response.[38] Following radiotherapy-induced cell death, cells released their DNA and RNA sensed by immune cells via a multitude of nucleic acid-recognition pathways. Of these, the cyclic GMP–AMP synthase (cGAS) stimulator of interferon genes (STING) pathway is considered of key importance to the propagation of radiotherapy-induced immune responses leading to tumor control.[39,40] The radiosensitization of GONs is dose and concentration dependent. Whether the radiotherapy-induced immune responses can be reinforced by GONs? The specific impact of GONs on the intricacies of the tumor immune microenvironment needs to be elucidated. In this work, the precise in vivo distribution and metabolism of GONs were studied, deciphering the radiosensitization effect and the underlying biomechanisms of GONs in triple-negative breast cancer models under different radiation fractions. Based on our investigation, it has been observed that GONs possess the capability to induce apoptosis in 4T1 breast cancer cells by significantly augmenting the generation of ROS subsequent to irradiation, leading to heightened DNA damage within the 4T1 breast cancer cells. Moreover, within the in vivo tumor microenvironment, the synergistic application of fractionated X-ray irradiation and GONs can effectively trigger the activation of the cGAS-STING pathway, consequently fostering enhanced intratumoral infiltration and activation of downstream $CD8^+$ T cells. As a result, this combined approach exhibits superior efficacy in impeding the progression of 4T1 breast cancer. Our study shows that GONs are a potential theranostic reagent.

Methods and Materials

Synthesis of GONs

Gadolinium(III) nitrate hexahydrate ($Gd(NO_3)_3•6H_2O$, 99%), diethylene glycol (DEG, 99%), and sodium hydroxide (NaOH, 99%) were all purchased from Aladdin Industrial Inc. (Shanghai, China). GONs were synthesized following a previously reported method.[26] Briefly, 26 mL 0.1 g/mL Gd $(NO_3)_3•6H_2O$ in DEG was heated to 100 °C with vigorous stirring. After that, 34 mg NaOH solution in 34 mL DEG was added into the Gd $(NO_3)_3•6H_2O$ solution drop by drop slowly. After refluxed 60 min at 140 °C, the temperature of the mixture was raised to 175 °C for another 4 h. The GON sample obtained was naturally cooled and purified by membrane dialysis with cut-off of 3500 Da for 72 h with Milli-Q water. The water was replaced with a fresh one every 8 h.

High-Resolution Transmission Electron Microscopy and Elemental Energy Spectrum Analysis

10.0 μL of the diluted dispersion of GONs was deposited on a copper carrier coated with an ultrathin layer of carbon film (Zhongjingkeyi Films Technology Co., Ltd, Beijing, China) and then dried in an ultraclean air system. High-resolution transmission electron microscope (TEM) image of GONs was obtained from a Tecnai F30 (FEI, the Netherlands) instrument conducted at 300 kV. Elemental energy spectrum analysis was performed on the same apparatus by selecting a region of interest (ROI).

Relaxation Time Measurements and MRI

A small animal magnetic resonance scanner with a 1.0 T magnetic field (OPER-1.0, NingBo ChuanShanJia Electrical and Mechanical Co., Ltd, China) was applied to perform MRI on GONs in vitro and in vivo. OPER-1.0 was applied to determine the T_1 and T_2 relaxation time of GONs, and the relaxation rates ($r = 1/T$) were then linearly fitted to the concentration of nanoparticles.

Cell Culture

Murine breast cancer cell-line 4T1 was purchased from the Type Culture Collection of the Chinese Academy of Sciences (Shanghai, China). 4T1 cells were cultured in RPMI 1640 medium (Meilun, China) with 10% fetal bovine serum (Lanzhou Minhai Bio-Engineering, China) in an incubator with carbon dioxide content of 5% at a constant temperature of 37 °C.

Tumor-Bearing Mice

Female Bal/bc mice with a weight of 16–17 g were purchased from the experimental animal center of Lanzhou Veterinary Research Institute, Chinese Academy of Agricultural Sciences (Lanzhou, China). All research projects that require animals in this study were approved by the Animal Ethics Committee of the Institute of Modern Physics, Chinese Academy of Sciences (IMP-CAS No. 2022–10). 4T1 cells were used to establish a tumor-bearing animal model. 1×10^5 4T1 cells were injected into each mouse for subcutaneous tumor bearing. Vernier calipers were used to measure the length (L) and width (W) of mouse tumors and calculate the volume (V) of mouse tumors with the following formula:[41] $V = 0.5 \times L \times W^2$.

X-Ray Irradiation

All in vitro and in vivo irradiation experiments were performed on an X-RAD 225 X-ray irradiation apparatus (Precision Co., Ltd., USA) operated at 225 kV and 13.3 mA. The source-skin distance (SSD) for radiotherapy was set to 50 cm. Local X-ray irradiation (8.0 Gy × 1 Fr or 3.0 Gy × 3 Fr) was performed on the tumor site of each mouse. Mice in different groups were injected intratumorally with 50 μL of sterile water or 50 μL of GONs (8 mM) 10 minutes before irradiation.

Cell Counting Kit-8 (CCK-8) Assay

We used the previously reported method for CCK-8 experiments.[30] On the first day, 4T1 cells were planted in a 96-well plate (100 μL of medium containing 5000 cells per well) and cultured for 24 h. The next day, the culture medium was discarded, and culture medium containing different concentrations of GONs was added to co-culture with the cells for 24 h. On the third day, the medium was discarded again, and the medium containing CCK8 reagent (10%) was added and incubated at 37°C. The optical density (OD) at 450 nm of the sample well of 96-well plate was detected with a microplate reader (Tecan infinite M200 plex, Männedorf, Switzerland) at 0.5, 1.0 and 2.0 hours, respectively. Cell viability is calculated using the following formula:

$$Cell\ viability\ = \frac{OD_X - OD_0}{OD_C - OD_0}$$

where OD_X is OD value of wells containing cells after 24 h of co-cultivation with GONs; OD_C is OD value of wells containing cells after 24 h of co-cultivation in GONs-free medium; OD_0 is OD value of wells containing only CCK8 reagent medium without cells.

Clonogenic Survival Assay

The previously published method of cloning survival assay was employed in our study.[42] Cells from different treatment groups were grown in quadruplicate in a 60 mm diameter petri dish. The survival rate (SF) was calculated by comparing the planting efficiency (PE) of the treatment group with that of the control group.

$$\mathrm{PE}\ = \frac{\text{Number of colonies counted}}{\text{Number of cells plated}} \times 100\%$$

$$\mathrm{SF}\ = \frac{\text{PE of treated sample}}{\text{PE of control}} \times 100\%$$

The cells were digested and collected by X-ray irradiation of 225 kV with a dose of 0, 1.0, 2.0, 4.0, and 6.0 Gy, respectively, then diluted and planted in petri dishes with a diameter of 60 mm (the number of planted cells was 200, 300, 400, 700, and 2000 cells/dish). The incubators for culturing clonally viable cells were individually dedicated. After ten

days of culture, the medium was discarded and the residual medium was washed off with PBS, and the prepared crystal violet solution was dyed for 20 minutes. Finally, the dye was recovered, and the residual dye was slowly washed away with flowing water. An inverted microscope was used to observe and count the number of colonies, and a cluster of blue-staining cells including at least 50 cells were defined as a colony. The cell survival data were fitted with a linear quadratic (LQ) model, and the sensitization enhancement ratio of GONs was evaluated under the conditions of 50% and 20% cell survival rates.

Flow Cytometry

4T1 cells were digested and collected with EDTA-free trypsin (Solarbio life science, Beijing, China) 24 h after irradiation with X-rays. The cells were washed twice more with pre-chilled PBS, then resuspended with staining buffer, and finally PI (5 μL per sample) and AnnexinV FITC (10 μL per sample) were added for 15 min before machine detection. Apoptosis detection kits (#E-CK-A211) were purchased from Multisciences Biotech, CO., LTD (Beijing, China). The FlowJo software was used to analyze the data obtained by flow cytometry.

Immunofluorescence and Immunohistochemistry

Antibodies or regents: Mounting medium, antifading (with DAPI, S2110, Solarbio life science), phospho-histone H2A.X (Ser139) (20E3) Rabbit mAb #9718 (Cell Signaling Technology (CST), Massachusetts, USA), Dylight 649, Goat Anti-Rabbit IgG (#A23620, Abbkine, Wuhan, China) and DAB (SA-HRP) Tunel Cell Apoptosis Detection Kit (#G1507-50T, Servicebio, Wuhan, China) were used. A laser confocal microscope (LSM700 Laser Confocal Microscope, Zeiss, Oberkochen, Germany) was used for observation and picture acquisition.[43,44]

Reactive Oxygen Species Assay

Reactive oxygen species kit was purchased from Solarbio Life Science (Beijing, China) and operated according to the instructions. CFH-DA was diluted with serum-free medium at 1:1000 to a final concentration of 10 μmol/L. 4T1 cells from different treatment groups were collected and suspended in diluted DCFH-DA at a concentration of 1 million cells per mL and incubated for 20 min in an incubator at 37 °C. Cells were mixed upside down every 3–5 min to allow sufficient contact between the probes and cells. The cells were washed three times with serum-free medium to fully remove the DCFH-DA that had not entered the cells. 10,000 cells per well were added to a 96-well plate with each assembled fluorescent probe, and 5 wells were repeated for each group. The fluorescence intensity of each well was then detected by microplate reader and finally averaged to each cell.

Western Blot

Cells were first lysed using RIPA Lysis Buffer (containing 1% protease and phosphatase inhibitors). Centrifuge at 13000 g for 15 min at 4 °C, collect protein samples from the supernatant, and perform protein quantification by BCA method. The target protein and the carrier protein buffer are mixed according to the ratio of 3. After boiling for 10 minutes, an equal amount of sample was loaded on 10% SDS-PAGE separation gel and electrophoresed (S1 80 V for 20 mins, S2 120 V 90 mins). Next, the proteins were transferred to a polyvinylidene fluoride (PVDF) membrane (constant current 150 mA, 150mins) and blocked with rapid blocking solution for 30mins at room temperature according to the reagent manufacturer's instructions. Membranes were then incubated with primary antibody (cGAS, STING, pSTING, Actin) overnight at 4 °C, followed by secondary antibody incubation for 60 mins. Finally, ECL system was used for exposure and color development, and ImageJ was used for image processing. Primary or secondary antibodies, including cGAS (D3O8O) Rabbit mAb (CST, #31659), STING (D2P2F) Rabbit mAb (CST, #13647), Phospho-STING (Ser365) (D8F4W) Rabbit mAb (CST, #72971) and HRP* Goat Anti Rabbit IgG(H+L), ImmunoWay Biotechnology Company (TX,75024 USA), #RS0002, were used.

Real-Time Quantitative PCR

Total RNA was extracted from 4T1 cells by RNA extraction kit (RNAeasyTM Animal RNA Isolation kit with Spin Column), and the RNA concentration was measured by NANO Drop (Thermo Fisher Scientific). The RNA was then

quantified to 1000 ng, and the RNA was transcribed using a reverse transcription kit (PrimeScript RT Master Mix (Perfect Real Time), Takara, Cat. No. RR036A). 20 μL of the system was reverse-transcribed into cDNA, and 80μL of water was added to dilute the transcribed cDNA. Finally, PCR was performed using a PCR kit (GoTaq qPCR Master Mix: Promega, Cat. No. A6002), PCR reaction was carried out according to the operation steps to detect the expression of related genes at mRNA level in different treatment groups. Primer sequences were synthesized by Sangon Biotech Co., Ltd. (Shanghai, China).

TBK1,
Forward primer: ATCAAGAAGGCACGCATCCA,
Reverse primer: GGCTCATTGCTTTTGTGGCA;
IRF3,
Forward primer: GCTGAGGTCTAGGTGCTCCA
Reverse primer: GTGACAGTGTCCCTTGCTCC
GAPDH,
Forward primer: CCTCGTCCCGTAGACAAAATG
Reverse primer: TGAGGTCAATGAAGGGGTCGT

Statistical Analysis

Each experiment was carried out in triplicate except for special cases, and the data presentation of a single experiment includes all parallel repeated data. The statistical significance between the different groups was assessed using a two-tailed Student's *t*-test and one-way analysis of variance (ANOVA), which was performed in the SPSS 19.0 software. P value < 0.05 was considered significantly different.

Results

Characterization of GONs

Engineering GONs by a polyol method, we prepared the sample for electron microscope observation with GON's diluent. The high-resolution TEM images of GONs are shown in Figure 1A–C, where regular crystal patterns could be observed with lattice spacing of 0.31 nm measured by GATAN Digital Micrograph (Version 3.40.2804.0), as shown in Figure S1A. The particle size of the crystal nucleus of the nanoparticles was about 3–4 nm. The energy-dispersive spectroscopy (EDS) analysis of GONs is shown in Figure 1D and E. In the EDS spectrum, the peaks at about 530 eV and 1.22 keV corresponded to O (*1s*) and Gd (*3d*) in Gd_2O_3 nanoparticles, respectively. The K emission line of oxygen appeared at about 200 eV. The L-emission line of Gd emerged at around 6.0 keV. Gadolinium and oxygen were contained in the synthesized GONs. The results obtained by TEM are consistent with the previous studies[26,29] and also have good agreement with the cubic crystal phase of Gd_2O_3.

MRI of GONs in vivo and in vitro

T_1- and T_2-weighted MRI images were obtained by in vitro imaging of GONs at different concentrations on a small animal magnetic resonance device with a primary magnetic field strength of 1.0 T (Figure 2A and B). Moreover, the T_1 and T_2 relaxation times of various GONs were quantified, and subsequent calculation of the relaxation rate ($r = 1/T$) of GONs was performed based on the measured relaxation times (Figure S1B–C). A significant linear correlation has been observed between the concentration of nanoparticles and the magnetic relaxation rate (r) using the equation $r = kC + b$ (Figure 2C and D). The calculated value of r_2 / r_1 was 2.69, indicating that the synthesized GONs possess excellent potential as a positive MRI contrast agent.[45] Specifically, we undertook a comprehensive MRI investigation of GONs distribution and metabolism in mice, which enabled us to precisely monitor the nanoparticle distribution in the animals (Figure 2E). Analysis of the MRI signal revealed that GONs maintained a steady concentration within the tumor, even 120 minutes after injection (Figure 2F). The four small circular areas around the mouse body represented tubes containing nano-solutions of different concentrations, thus giving a relative in vitro reference to the signal changes of GONs in vivo. From the MRI images, it was observed that GONs were primarily cleaned by the kidney, with renal signal

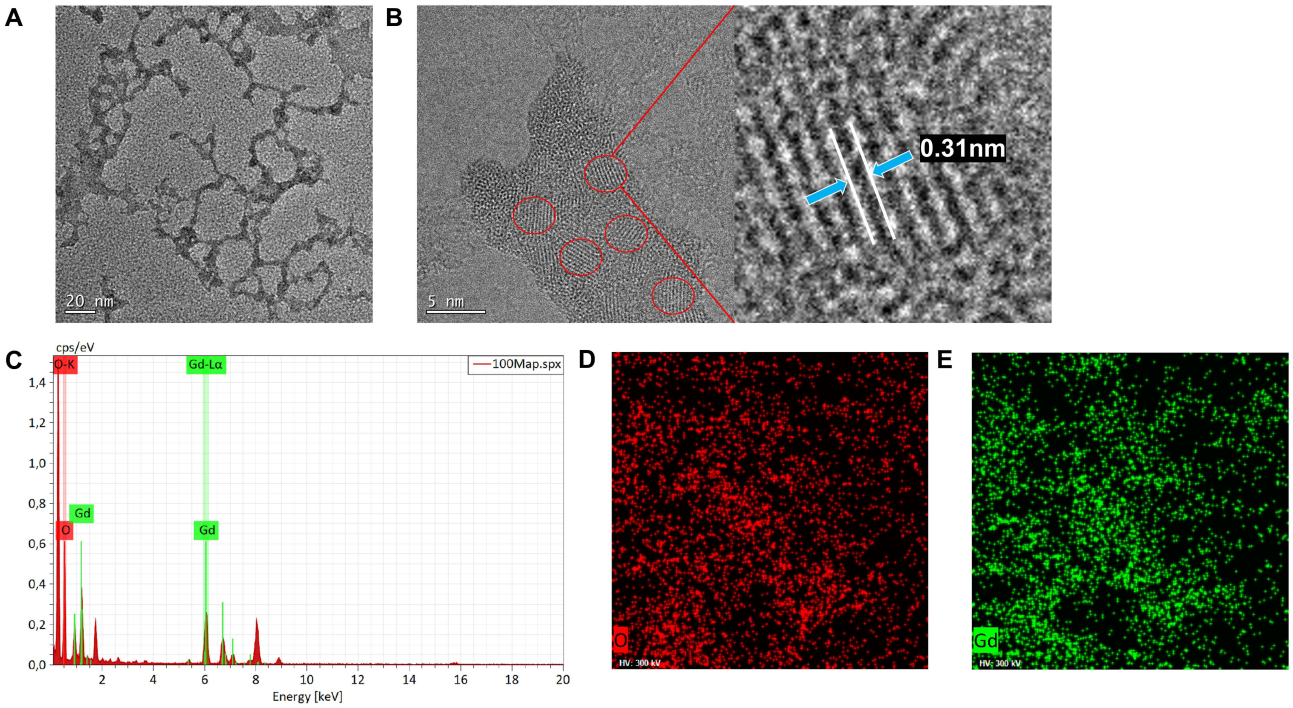

Figure 1 Characterization of GONs. The electron microscope images of GONs at 20 nm (**A**) and 5 nm (**B**) scales, where the lattice structures could be seen in the images. Partially enlarged nanocrystal image when measuring lattice spacing with the GATAN Digital Micrograph software. In Figure B, each nanocrystal particle is circled in red; the blue arrow indicates a lattice spacing between two white lines. (**C**) Characterizing the elemental composition of nanoparticles with EDS. (**D**) The distribution of oxygen elements in the field of electron microscope at the red pixel, and the distribution of gadolinium (**E**) in the field of electron microscope at the same green pixel. The distribution of the energy spectrum peaks of oxygen and gadolinium could also be obtained from the images.

starting to increase at 5 minutes after injection (Figure 2G). Remarkably, GONs were not found to accumulate in the liver of mice (Figure 2H). Collectively, the results of the present study demonstrated that GONs exhibit desirable characteristics as a T_1-weighted MRI contrast agent, with no concurrent toxic effects identified.

Radiosensitizing Effect of GONs to X-Ray Irradiation in vitro

The present investigation employed the CCK-8 assay to assess the viability of 4T1 cells co-cultured with various concentrations of GONs (Figure 3A). Our results indicated that exposure to diverse concentrations of GONs did not induce any significant inhibitory effect on the proliferation of 4T1 cells when compared to the control groups, indicating the absence of toxic effects induced by GONs on 4T1 cells. Toxicity tests for GONs were also conducted in vivo, as illustrated (Figures S2A–O and S3A–G). It was observed that when 10 mM GONs were injected via the tail vein in a volume of 200 μL, no significant impact on the body weight of mice was detected, and there were no evident toxic side effects observed on vital organs such as the heart, spleen, lungs, and kidneys. Additionally, HE staining revealed no signs of organ damage in the mice one month after the injection of GONs. Furthermore, the survival fraction of 4T1 cells was evaluated under X-ray irradiation both in the presence and absence of GONs, where the Gd concentration in the culture medium was set at 5.0 and 50.0 μg/mL. The survival data were assessed using a linear quadratic (LQ) model[29] (Figure 3B and C). Clonogenic assays revealed that GONs could effectively enhance the sensitivity of 4T1 cells to X-ray irradiation. The sensitizer enhancement ratio (SER) of GONs was calculated using the method reported in the literature.[29] As delineated in Table 1, it was observed that adding 5.0 μg/mL of gadolinium (Gd) demonstrated a more pronounced radiosensitization effect on 4T1 cells compared to the effect exhibited by 50.0 μg/mL of Gd. Henceforth, the subsequent cell experiments employed the usage of 5.0 μg/mL Gd. Calculated by fitting equations, the SERs of GONs at 5.0 and 50.0 μg/mL Gd concentrations were 73% and 70% at 50% survival fraction level, respectively.

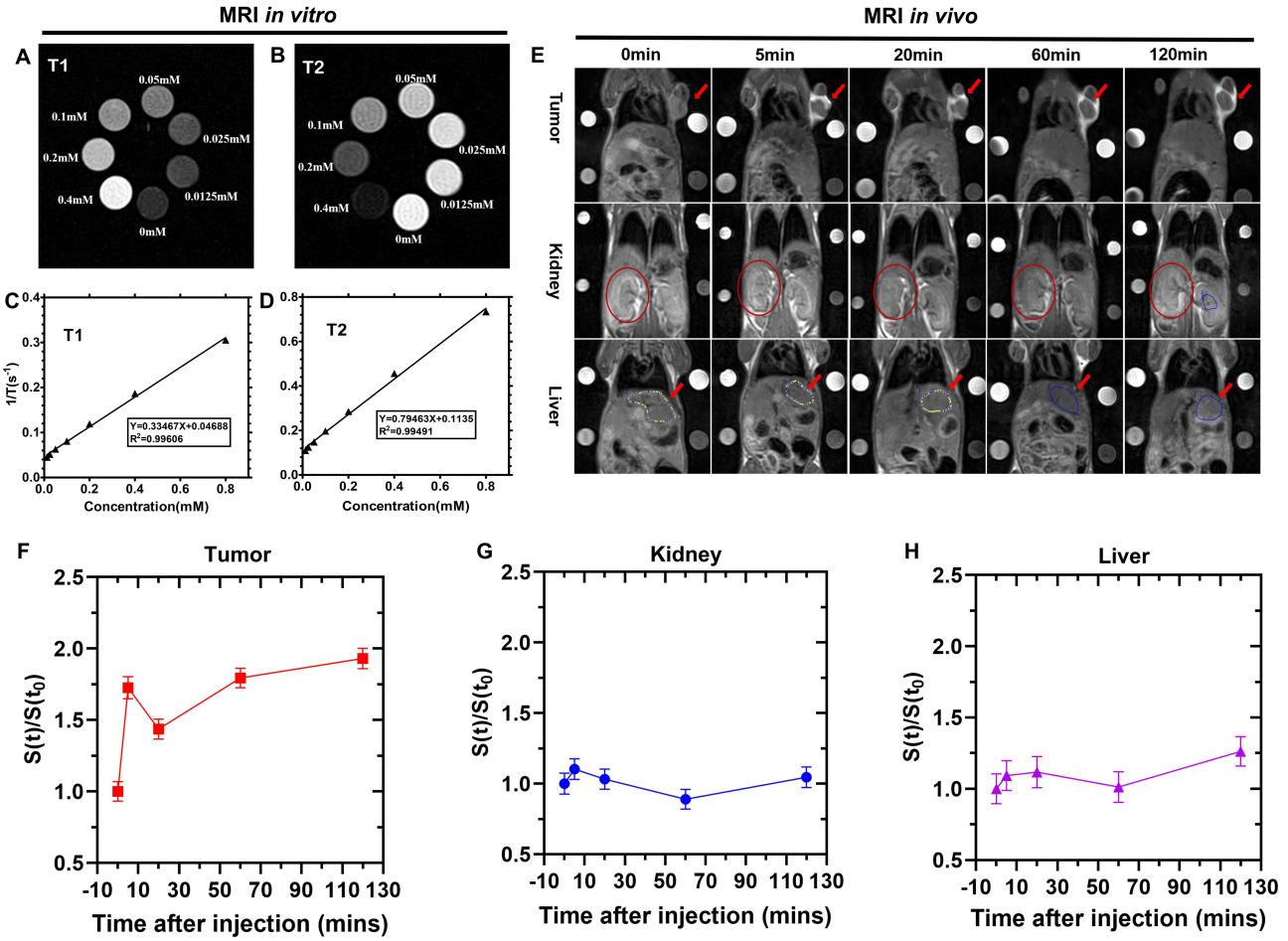

Figure 2 T_1-weighted imaging (**A**) and T_2-weighted imaging (**B**) of different Gd concentrations of nanoparticles with 1.0T magnetic resonance equipment. The linear fit of T_1 (**C**) and T_2 relaxation rates (**D**) of nanoparticles with different concentrations versus concentration and the equation of the relationship. (**E**) T_1-weighted magnetic resonance images of different organs and tumors in mice within 2 hours after nanoparticle injection. The first row of red arrows after the tumor heading is where the mouse tumor is; the second row of red circles is where the mouse kidney is; the third row of red arrows is where the mouse liver is; we have drawn the ROI (Region of interest). (**F**–**H**) The T_1 magnetic resonance signal intensity at different time points was also measured.

To elucidate the potential mechanisms underlying the enhancement of 4T1 cells' sensitivity induced by GONs, we initially assessed the levels of reactive oxygen species (ROS) presented in the distinct treatment groups. The results revealed that the addition of GONs significantly increased the level of ROS in irradiated 4T1 cells (Figure 3D). Furthermore, the double-stranded DNA breakage induced by GONs combined with X-rays, 1 hour after irradiation, was approximately 52% greater than that caused by irradiation alone (Figure 3E and F). The observed results of the DNA damage assay were consistent with those of the intracellular ROS production in 4T1 cells. Moreover, flow cytometry was used to determine the apoptotic rate of 4T1 cells following irradiation. The results demonstrated that the rate of apoptosis in irradiated cells was 1.5 times higher in the presence of GONs, 24 hours post-irradiation, than in cells irradiated in the absence of GONs (Figure 3G and H). Taken together, these findings suggested that GONs enhanced the apoptosis of tumor cells by upregulating the generation of reactive oxygen species, leading to increased DNA damage, which ultimately resulted in the sensitization effect of GONs under X-ray irradiation (Figure 3I).

Radiosensitizing Effect of GONs to X-Ray Irradiation in vivo

To validate the radiosensitization effect of GONs in vivo, we established a subcutaneous xenograft model of 4T1 breast cancer. Following the successful MRI study of tumor-bearing mice treated with GONs (Figure 2E), we conducted further in vivo experiments on the radiation enhancement capacity of GONs by administering them via intratumoral injection. Subsequently, X-ray irradiation was administered within 10 minutes after the injection mentioned above (MRI of GONs

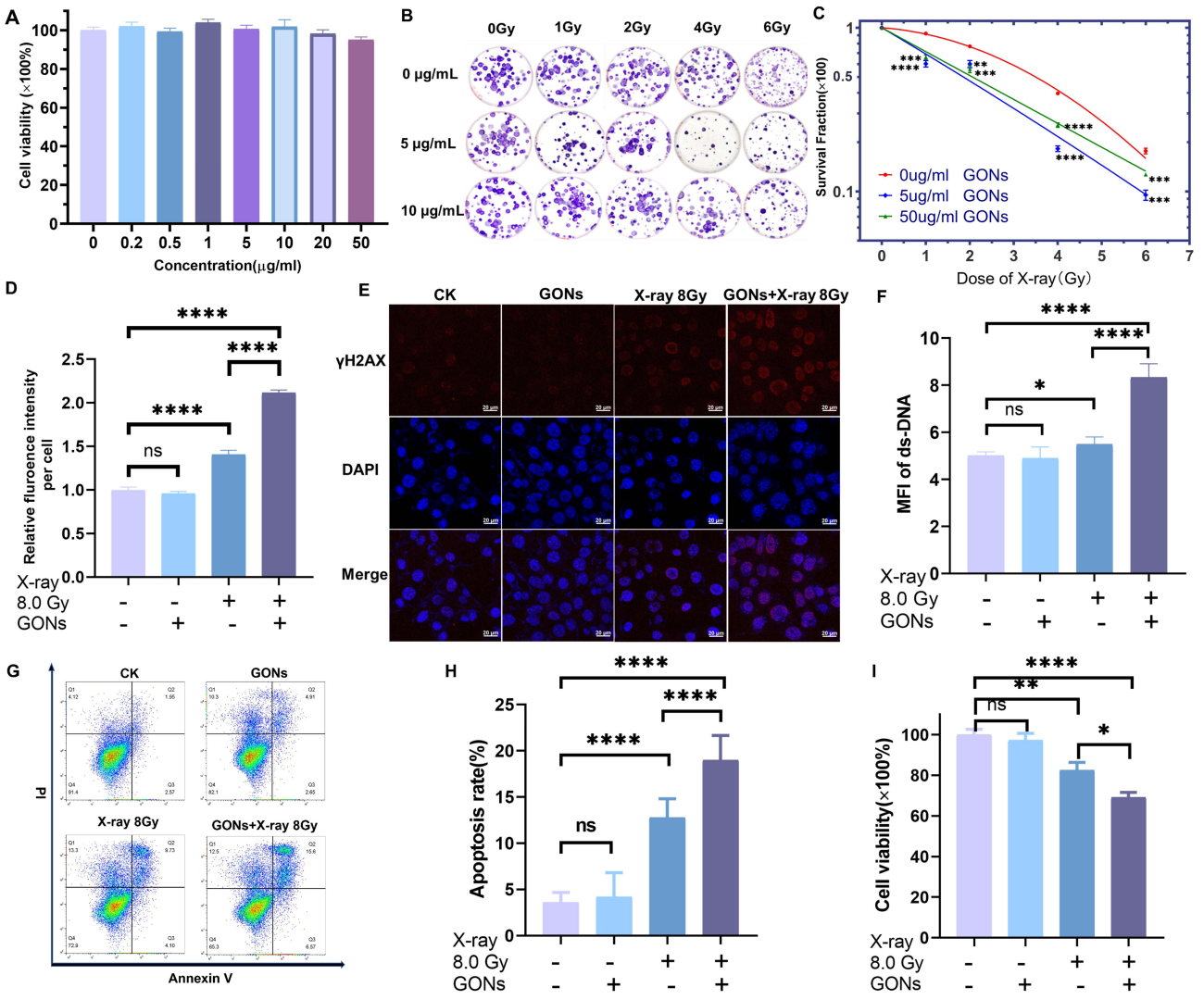

Figure 3 Effect of GONs pre-treatment on the cellular sensitivity to X-ray irradiation. (**A**) Detection of cell viability of different concentrations of gadolinium oxide nanoparticles on 4T1 cells after co-incubation proved. (**B**) Survival array of clones obtained by incubating GONs at different concentrations for 24 h and then X-ray irradiation. (**C**) By counting the number of clonal spots in different treatment groups, the survival rate of different treatment groups was calculated from this data and fitted with the linear quadratic model. (**D**) Detection of reactive oxygen species in different treatment groups. (**E**) Double-stranded DNA breaks in different treatment groups at 1 h after irradiation were detected by immunofluorescence. Red fluorescence is DNA damage foci labeled by γH2AX and blue fluorescence is nuclei labeled by DAPI. All the scale bars in the figure are 20 μm. (**F**) The average fluorescence intensity of double-stranded DNA damage in different treatment groups was obtained by quantifying the images obtained by laser confocal microscopy with ZEN 2.3. (**G**) Representative images of apoptosis in different treatment groups 24h after irradiation, and the (**H**) statistical graph of apoptosis ratio in different treatment groups. (**I**) Cell viability of cells in different treatment groups. (**C, D, F** and **I**) Data quantifications were analyzed using a Student's *t*-test and expressed as mean ± s.e.m, *p < 0.05, **p < 0.01, ***p < 0.001, ****p < 0.0001, ns means not significant.

in vivo and in vitro)(Figure S4). In our study, we administered a single dose of 8.0 Gy X-rays for local irradiation of tumors in mice. Unexpectedly, the group that received the combination treatment did not show a significant inhibition of tumor growth nor an extension of the lifespan of the animals, when compared to the group that received the radiation

Table 1 Summary of the Fitting Parameters, D_{20}, D_{50}, SER_{20}, SER_{50} for 4T1 Cells Under X-Ray Irradiation in the Absence/Presence of GONs

X-Ray Irradiation	α	β	R^2	D_{20} (Gy)	SER_{20}	D_{50} (Gy)	SER_{50}
Control	0.0466	0.043	0.998	5.55		3.5	
5.0 μg / mL Gd	0.337	0.0093	0.953	4.24	31%	2.02	73%
50.0 μg / mL Gd	0.336	0.0010	0.999	4.68	19%	2.06	70%

Note: Coefficients α, β, and R^2 are the fitting parameters using the linear-quadratic model; D_{20} and D_{50} mean the dosage of X-ray irradiation at 50% cell survival fraction; SER_{20} and SER_{50} mean sensitizer enhancement ratios of irradiated 4T1 cells at 20% and 50% cell survival fraction.

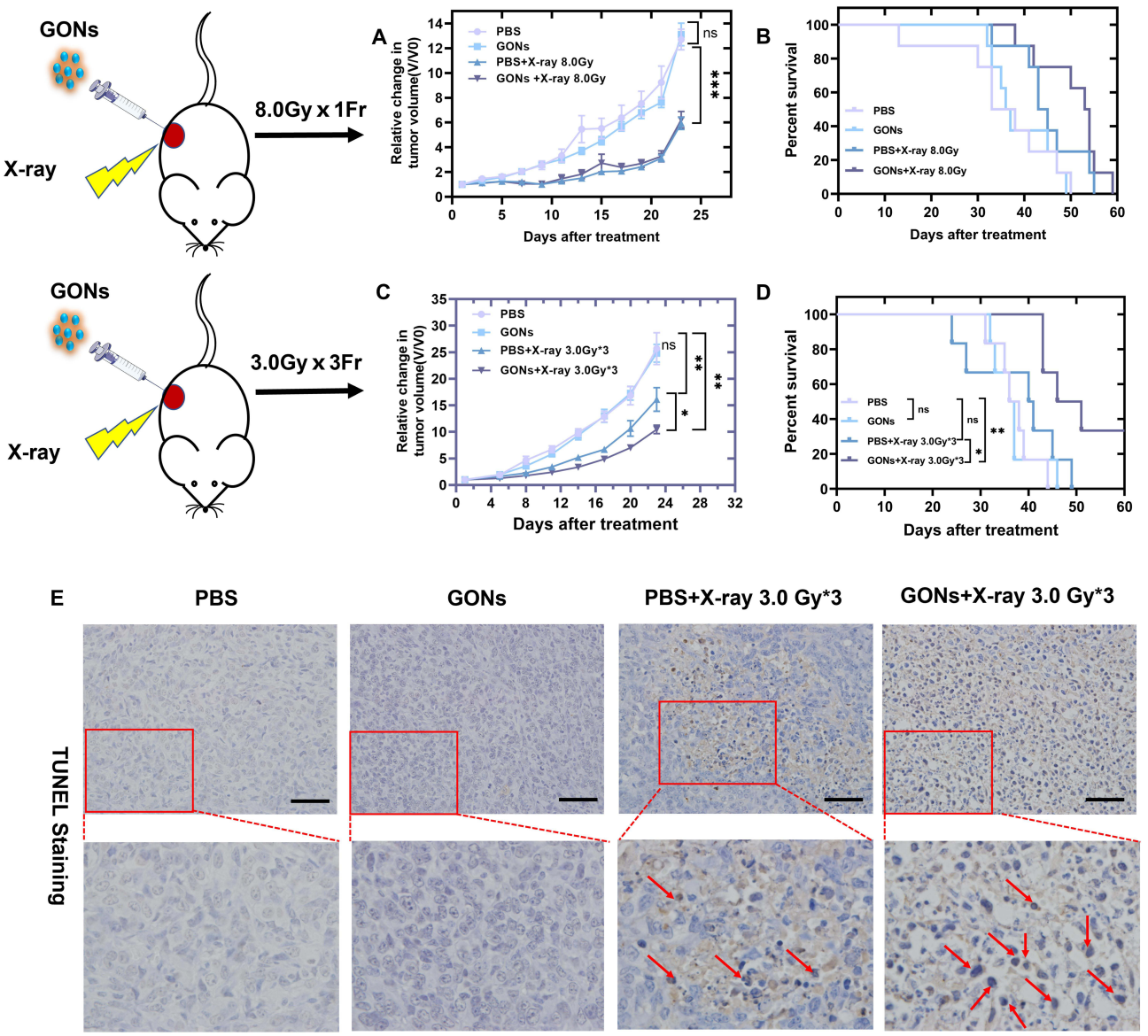

Figure 4 Radiation sensitization effect of GONs in vivo. Tumor growth curve (**A**) and survival curve (**B**) of mice in fractionated 8.0 Gy irradiation experiment. Tumor growth curve (**C**) and survival curve (**D**) of mice in fractionated 3.0 Gy*3 irradiation experiment. Data quantifications were analyzed using a Student's *t*-test (**A** and **C**) or a Log-rank (Mantel-Cox) test (95% CI) (**B** and **D**) and expressed as mean ± s.e.m, *p < 0.05, **p < 0.01, ***p < 0.001, ns means not significant. (**E**) Tunel staining of tumors in the different treatment groups. All the scale bars in the figure are 100 μm. The red arrows point to cells that are Tunel-positive for apoptosis.

treatment alone (Figure 4A and B). This observation deviates from our in vitro studies. Accordingly, we modified our radiation regimen to 3.0 Gy X-rays administered in three fractions separated by a 24-hour interval. Remarkably, the use of fractionated irradiation with GONs exhibited a significant inhibitory effect on 4T1 tumors while simultaneously prolonging the survival time of mice, which is a promising finding worthy of further investigation (Figure 4C and D). By utilizing TUNEL staining to examine the spatial distribution of apoptotic cells within the tumor, our study revealed that the use of GONs significantly enhanced apoptosis in 4T1 breast cancer cells following fractionated irradiation (Figure 4E). Since 4T1 cells are reported as strongly metastatic tumor cells, the mice in each treatment group were sacrificed to observe the tumor metastasis in the lungs of the mice. We found that neither single-dose irradiation nor fractionated irradiation combined with GONs exhibited superior efficacy in inhibiting lung metastasis of 4T1 tumors (Figure S5A–D). Throughout the duration of the experiment, a systematic and ongoing monitoring of each mouse's weight was conducted, and there was no significantly statistical difference in the weight of the mice across all the

treatment groups (Figure S5E and F). The aforementioned findings also provided evidence for the safety of using GONs in mouse treatment, as there was no discernible distinction between the PBS and GONs treatment groups. Remarkably, upon conducting identical treatment in immunodeficient mice, the previously observed radiosensitizing benefit of GONs was no longer prominent (Figure S6A–H). These findings substantiate the notion that the radiosensitizing impact of GONs is intricately linked to the activation of the anti-tumor immune system.

Immune Response Enhancement by GONs

Given the enhanced therapeutic efficacy of the combination of fractionated irradiation and GONs, it is of interest to explore the underlying reasoning for the superior performance of fractionated irradiation over single irradiation in the context of combination therapy in vivo. The intricate immune microenvironment in which tumor cells exist in vivo implies that the diverse immune system activation resulting from fractional versus single irradiation may lead to contrasting therapeutic outcomes.[46] Upon comparison, our analysis revealed that within the single 8.0 Gy X-ray irradiation mode, neither irradiation alone nor its combination with GONs treatment produced any discernible alterations in the related proteins involved in the cyclic GMP-AMP synthase-stimulator of interferon genes (cGAS -STING) pathway (Figures 5A and S7). In contrast, for the 3.0 Gy × 3Fr X-ray irradiation mode, our analysis showed that the irradiation alone significantly increased the expression levels of both cGAS and pSTING compared to the control group and the GONs alone treatment group. Remarkably, our analysis revealed that the combination of radiation with GONs treatment yielded maximum upregulation of the cGAS-STING pathway proteins (Figures 5D and S8). These outcomes suggested that the 3.0 Gy × 3 Fr X-ray irradiation combined GON therapy might more effectively activate anti-tumor immune responses, which is also in accordance with results observed in vivo study.

In addition, we conducted an examination of downstream associated molecules at the mRNA level by utilizing RT-qPCR. Our findings demonstrated that a single dose of 8.0 Gy X-ray irradiation combined with GONs treatment elicited a significant increase in the expression of TBK1. However, no significant difference was observed when compared with the irradiation alone (Figure 5B). Furthermore, of particular interest was the reduction in IRF3 expression at 8.0 Gy X-ray irradiation, and the reduced expression was more pronounced in the combination group than in the irradiation alone group (Figure 5C), suggesting that the ultimate consequence of single irradiation was the suppression of anti-tumor immune responses. The apparent upregulation in the expression levels of TBK1 (Figure 5E) and IRF3 (Figure 5F), as observed with the combined use of GONs and 3.0 Gy × 3 Fr X-ray irradiation, is a promising result. By immunohistochemical staining, we found more $CD8^+$ T cells infiltrating into the tumors in the combination group (Figure 5G). Such findings lend credence to the notion that GONs and fractionated irradiation implemented in conjunction may serve as a more potent means of stimulating anti-tumor immune responses.

Discussion

There are many kinds of metal-based nanoparticles used for ionizing radiation sensitization, such as gold-based nanoparticles,[7,47,48] iron-based nanoparticles,[49,50] platinum-based nanoparticles[51] and gadolinium-based nanoparticles.[5,20,22,23] Recent studies have shown that gadolinium-based nanoparticles have significant potential for clinical application as they can be utilized as both MRI contrast agents and radiosensitizers to improve tumor killing. There exists a wide variety of metal-based nanoparticles employed for the purpose of sensitizing ionizing radiation, inclusive of gold-based, iron-based, platinum-based, and gadolinium-based nanoparticles. Despite gold-based and platinum-based nanoparticles demonstrating commendable efficacy as radiation sensitizers, their utilization entails higher production costs owing to their association with noble metals. In contrast, iron-based nanoparticles are frequently utilized as T_2 contrast agents in magnetic resonance imaging (MRI) due to their magnetic properties, causing a reduction in T_2 signal intensity during imaging. Notably, MRI offers the advantage of not administering additional radiation as compared to CT imaging, where gold-based and platinum-based nanoparticles can be employed as contrast agents. Consequently, GONs present favorable attributes of cost-effectiveness and integration of diagnosis and treatment, thus differentiating them from alternative nanoparticle types. More specifically, we aimed to evaluate the effect of GONs on the survival fraction of 4T1 cells, subjected to different fractional X-ray irradiation, using clonogenic survival assay as a measure of effectiveness. After checking the retention time of GONs in tumor-bearing mice using MRI, we studied the tumor growth

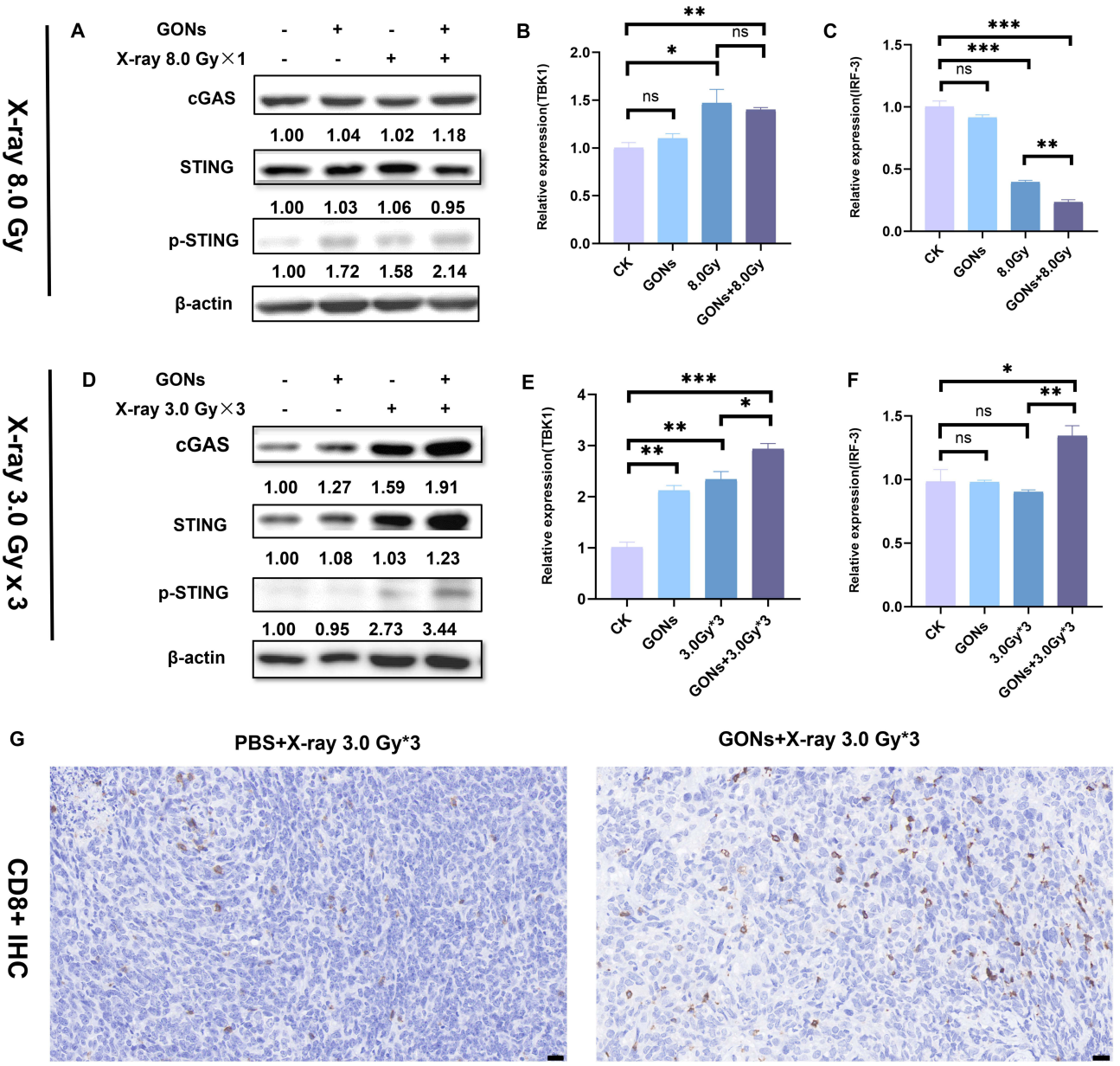

Figure 5 Western Blot was used to detect the expression of proteins associated with cGAS-STING signaling pathway. RT-qPCR was used to detect the expression of downstream signaling molecules TBK1 and IRF3. (**A**) WB bands and relative expression of cGAS-STING related proteins in different treatment groups in single 8.0Gy irradiation test. Relative mRNA expression levels of TBK1 (**B**) and IRF3 (**C**) in different treatment groups in a single 8.0 Gy irradiation test. (**D**) WB bands and relative expression of cGAS-STING related proteins in different treatment groups in fractionated 3.0 Gy*3 irradiation test. Relative mRNA expression levels of TBK1 (**E**) and IRF3 (**F**) in different treatment groups in fractionated 3.0 Gy*3 irradiation test. (**B, C, E** and **F**) Data quantifications were analyzed using a Student's *t*-test and expressed as mean ± s.e.m, *p < 0.05, **p < 0.01, ***p < 0.001, ns means not significant. (**G**) The distribution of CD8+T cells in tumor tissues of mice treated with GONs and irradiation alone. All the scale bars in the figure are 20 μm.

and survival time of tumor-bearing mice under the combination treatment of GONs and X-ray irradiation. Further, we studied the immune response of combination treatment in order to demonstrate the potential use of GONs as theranostic agent in breast cancer radiotherapy. In previous studies, our team also found the concentration-dependent radiosensitization effect of GONs in non-small cell lung cancer in vitro, and revealed the radiosensitizing biomechanism of GONs under X-ray irradiation and carbon ion irradiation.[29,30] This work established that the combined use of GONs and X-ray irradiation contributes to the enhanced inhibition of clone formation of 4T1 cells, whilst impeding their proliferative ability. Notably, further studies have shown that the primary mechanism behind GONs' ability to boost X-ray irradiation

damage lies in their capacity to induce apoptosis in tumor cells by heightening the DNA damage that X-rays inflict upon 4T1 cells.

In in vivo trials, MRI revealed the distribution and metabolism of GONs in mice to determine the irradiation time after intratumoral injection of nanoparticles. Through the signal variation of MRI, we can ensure that the co-treatment results of X-ray irradiation after 10 minutes of intratumoral injection of GONs are reliable. Hence, GONs improved the real-time imaging of tumor in mice, which also provides a non-invasive new method for drug pharmacokinetics research.[52] Two radiation modes were employed, specifically single 8.0 Gy × 1Fr X-ray irradiation and fractional 3.0 Gy × 3 Fr X-ray irradiation. The outcomes demonstrated that only the fractional X-ray irradiation combined with GONs showed significant enhancement of the inhibitory effect of RT on tumor growth. This could be attributed to the superior capability of fractional irradiation in activating anti-tumor immune responses in animals,[53] so GONs may increase the killing of tumor cells by the immune system by enhancing the antigen release after irradiation of 4T1 tumors. Simultaneously, it has also been reported that tumors in vivo have a more complex immune microenvironment, which has caused inconsistent results in vitro and in vivo experiments.[46] The cGAS-STING pathway is a crucial innate immune pathway, triggered by DNA and elicits a diverse range of immune responses that exert an influence on multiple facets of tumorigenesis, encompassing malignant cell transformation as well as metastasis.[54] Although there are several damage-associated molecular patterns that can activate innate immune mechanisms in the context of cancer, the aberrant recognition of DNA by the cGAS-STING pathway is especially pertinent to the endogenous detection of transformed or malignantly transformed cells, both in the basal state and after cancer treatment.[55] Thus, our inquiry has focused on scrutinizing cGAS-STING signaling pathway's role in facilitating anti-tumor immunity. Further investigation was conducted on the activation of GONs on the immune system, revealing that fractionated irradiation combined with GONs can trigger an anti-tumor immune response in animals through the activation of the cGAS-STING pathway. In contrast to previously documented gadolinium-based nanoparticles,[22–24] our investigation has unveiled a distinctive biological mechanism underlying the sensitization of GONs. This mechanism pertains to the modulation of the tumor immune microenvironment through the activation of the cGAS-STING pathway. Furthermore, our findings have also elucidated that diverse modes of irradiation elicit disparate sensitization mechanisms specific to gadolinium oxide nanoparticles. All aforementioned investigations have demonstrated that the incorporation of gadolinium oxide nanoparticles is correlated with diverse levels or divisions of radiation dosages in relation to the antitumor immune response.

Conclusion

Our study verified that GONs possessed favorable MRI contrast properties. Moreover, through the application of fractionated irradiation in conjunction with GONs, significant suppression of 4T1 breast cancer cells has been observed in vivo. This observed suppression was attributed to the activation of the cGAS-STING pathway, ultimately triggering an anti-tumor immune response. Thus, our study suggests that GONs have great potential to function as a comprehensive diagnostic and therapeutic tool for clinical application in MRI-guided radiotherapy.

Abbreviations

GONs, gadolinium oxide nanocrystals; MRI, magnetic resonance imaging; ROS, reactive oxygen species; EPR, enhanced permeability and retention; cGAS-STING, cyclic GMP-AMP synthase-stimulator of interferon genes; DSBs, double-stranded breaks; IGRT, image-guided radiotherapy; GdNPs, gadolinium-based nanoparticles; TEM, transmission electron microscope; CCK-8, Cell Counting Kit-8; EDS, energy-dispersive spectroscopy; SER, sensitizer enhancement ratio; LQ, linear quadratic; RT-qPCR, quantitative real-time PCR.

Ethics Approval

All animal experiments were approved by the Academic Committee of the Institute of Modern Physics, Chinese Academy of Sciences (No. 2022-10). All animal experiments were performed in the SPF class animal house at the Institute of Modern Physics, Chinese Academy of Sciences. We follow the "3R" principle in the experimental process, that is, the use of reduction, refinement and replacement methods in animal experiments, which is an important principle

to maintain the welfare of experimental animals. We also follow the National Institutes of Health (NIH) Guidelines for Laboratory Animal Welfare to ensure the welfare of laboratory animals.

Acknowledgments

We thank to Dr. Shixu Zhang (Lanzhou University, China) for his help in the characterization of GONs by electron microscopy, and Doctor Jinghui Li (NingBo ChuanShanJia Electrical and Mechanical Co., Ltd China) for his help in MRI sequence design. We are also grateful to Dr. Qingfeng Wu (Institute of Modern Physics, Chinese Academy of Sciences) for his help in applying the public shared instrument platform.

Funding

This work was jointly supported by the Key Deployment Project of Chinese Academy of Sciences [Grant No. KFZD-SW-222], the National Natural Science Foundation of China [Grant No. 82272746], the Natural Science Foundation of Gansu Province [Grant No. 21JR7RA106], the West Light Foundation of the Chinese Academy of Sciences [Grant No. xbzg-zdsys-201920] and the Natural Science Foundation of Gansu Province [Grant No. 23JRRA569].

Disclosure

The authors declare no conflicts of interest in this work.

References

1. Sung H, Ferlay J, Siegel RL, et al. Global cancer statistics 2020: GLOBOCAN estimates of incidence and mortality worldwide for 36 cancers in 185 countries. *CA-Cancer J Clin*. 2021;71(3):209–249. doi:10.3322/caac.21660
2. Barton MB, Jacob S, Shafiq J, et al. Estimating the demand for radiotherapy from the evidence: a review of changes from 2003 to 2012. *Radiother Oncol*. 2014;112(1):140–144. doi:10.1016/j.radonc.2014.03.024
3. Tyldesley S, Delaney G, Foroudi F, Barbera L, Kerba M, Mackillop W. Estimating the need for radiotherapy for patients with prostate, breast, and lung cancers: verification of model estimates of need with radiotherapy utilization data from British Columbia. *Int J Radiat Oncol Biol Phys*. 2011;79(5):1507–1515. doi:10.1016/j.ijrobp.2009.12.070
4. Post AEM, Smid M, Nagelkerke A, et al. Interferon-stimulated genes are involved in cross-resistance to radiotherapy in tamoxifen-resistant breast cancer. *Clin Cancer Res*. 2018;24(14):3397–3408. doi:10.1158/1078-0432.CCR-17-2551
5. Lux F, Tran VL, Thomas E, et al. AGuIX (R) from bench to bedside-transfer of an ultrasmall theranostic gadolinium-based nanoparticle to clinical medicine. *Br J Radiol*. 2018;92(1093):20180365. doi:10.1259/bjr.20180365
6. Candas-Green D, Xie BW, Huang J, et al. Dual blockade of CD47 and HER2 eliminates radioresistant breast cancer cells. *Nat Commun*. 2020;11(1):15. doi:10.1038/s41467-020-18245-7
7. Zhang P, Yu B, Jin X, et al. Therapeutic efficacy of carbon ion irradiation enhanced by 11-MUA-capped gold nanoparticles: an in vitro and in vivo Study. *Int J Nanomed*. 2021;16:4661–4674. doi:10.2147/IJN.S313678
8. Liu Y, Zhang PC, Li FF, et al. Metal-based Nanoenhancers for future radiotherapy: radiosensitizing and synergistic effects on tumor cells. *Theranostics*. 2018;8(7):1824–1849. doi:10.7150/thno.22172
9. Ahmad R, Royle G, Lourenco A, Schwarz M, Fracchiolla F, Ricketts K. Investigation into the effects of high-Z nano materials in proton therapy. *Phys Med Biol*. 2016;61(12):4537–4550. doi:10.1088/0031-9155/61/12/4537
10. Kuncic Z, Lacombe S. Nanoparticle radio-enhancement: principles, progress and application to cancer treatment. *Phys Med Biol*. 2018;63(2):02TR01. doi:10.1088/1361-6560/aa99ce
11. Kim J, Piao Y, Hyeon T. Multifunctional nanostructured materials for multimodal imaging, and simultaneous imaging and therapy. *Chem Soc Rev*. 2009;38(2):372–390. doi:10.1039/B709883A
12. Cui L, Her SY, Borst GR, Bristow RG, Jaffray DA, Allen C. Radiosensitization by gold nanoparticles: will they ever make it to the clinic? *Radiother Oncol*. 2017;124(3):344–356. doi:10.1016/j.radonc.2017.07.007
13. Her S, Jaffray DA, Allen C. Gold nanoparticles for applications in cancer radiotherapy: mechanisms and recent advancements. *Adv Drug Deliv Rev*. 2017;109:84–101. doi:10.1016/j.addr.2015.12.012
14. Keall PJ, Brighi C, Glide-Hurst C, et al. Integrated MRI-guided radiotherapy - opportunities and challenges. *Nat Rev Clin Oncol*. 2022;19(7):458–470. doi:10.1038/s41571-022-00631-3
15. Caravan P, Ellison JJ, McMurry TJ, Lauffer RB. Gadolinium(III) chelates as MRI contrast agents: structure, dynamics, and applications. *Chem Rev*. 1999;99(9):2293–2352. doi:10.1021/cr980440x
16. Le Duc G, Miladi I, Alric C, et al. Toward an image-guided microbeam radiation therapy using gadolinium-based nanoparticles. *ACS Nano*. 2011;5(12):9566–9574. doi:10.1021/nn202797h
17. Dufort S, Bianchi A, Henry M, et al. Nebulized gadolinium-based nanoparticles: a theranostic approach for lung tumor imaging and radiosensitization. *Small*. 2015;11(2):215–221. doi:10.1002/smll.201401284
18. Kotb S, Detappe A, Lux F, et al. Gadolinium-based nanoparticles and radiation therapy for multiple brain melanoma metastases: proof of concept before phase I trial. *Theranostics*. 2016;6(3):418–427. doi:10.7150/thno.14018
19. Lux F, Verry C, Dufort S, Tillement O, Le Duc G, Balosso J. Ultrasmall theranostic nanoparticles for the treatment of multiple brain metastases by radiation therapy: a first in man. *Int J Radiat Oncol Biol Phys*. 2017;99(2):E34–E34. doi:10.1016/j.ijrobp.2017.06.672

20. Bort G, Lux F, Dufort S, Crémillieux Y, Verry C, Tillement O. EPR-mediated tumor targeting using ultrasmall-hybrid nanoparticles: from animal to human with theranostic AGuIX nanoparticles. *Theranostics*. 2020;10(3):1319–1331. doi:10.7150/thno.37543
21. Aloy M-T, Sidi Boumedine J, Deville A, et al. Proof of concept of the radiosensitizing effect of gadolinium oxide nanoparticles in cell spheroids and a tumor-implanted murine model of chondrosarcoma. *Int J Nanomed*. 2022;17:6655–6673. doi:10.2147/IJN.S390056
22. Sun H, Cai H, Xu C, et al. AGuIX nanoparticles enhance ionizing radiation-induced ferroptosis on tumor cells by targeting the NRF2-GPX4 signaling pathway. *J Nanobiotechnol*. 2022;20(1):449. doi:10.1186/s12951-022-01654-9
23. Brown N, Rocchi P, Carmès L, et al. Tuning ultrasmall theranostic nanoparticles for MRI contrast and radiation dose amplification. *Theranostics*. 2023;13(14):4711–4729. doi:10.7150/thno.85663
24. Ren H, Hu Q, Yang J. et al. Single-molecule dendritic MRI nanoprobes reveal the size-dependent tumor entrance. *Adv Healthc Mater*;2023. e2302210. doi:10.1002/adhm.202302210
25. Ahren M, Selegard L, Klasson A, et al. Synthesis and characterization of PEGylated Gd2O3 nanoparticles for MRI contrast enhancement. *Langmuir*. 2010;26(8):5753–5762. doi:10.1021/la903566y
26. Ma XH, Gong A, Xiang LC, et al. Biocompatible composite nanoparticles with large longitudinal relaxivity for targeted imaging and early diagnosis of cancer. *J Mat Chem B*. 2013;1(27):3419–3428. doi:10.1039/c3tb20648c
27. Faucher L, Tremblay M, Lagueux J, Gossuin Y, Fortin MA. Rapid synthesis of PEGylated ultrasmall gadolinium oxide nanoparticles for cell labeling and tracking with MRI. *ACS Appl Mater Interfaces*. 2012;4(9):4506–4515. doi:10.1021/am3006466
28. Park JY, Baek MJ, Choi ES, et al. Paramagnetic ultrasmall gadolinium oxide nanoparticles as advanced T-1 MR1 contrast agent: account for large longitudinal relaxivity, optimal particle diameter, and in vivo T-1 MR images. *ACS Nano*. 2009;3(11):3663–3669. doi:10.1021/nn900761s
29. Li F, Li Z, Jin X, et al. Radiosensitizing effect of gadolinium oxide nanocrystals in NSCLC cells under carbon ion irradiation. *Nanoscale Res Lett*. 2019;14(1):328. doi:10.1186/s11671-019-3152-2
30. Li FF, Li ZH, Jin XD, et al. Ultra-small gadolinium oxide nanocrystal sensitization of non-small-cell lung cancer cells toward X-ray irradiation by promoting cytostatic autophagy. *Int J Nanomed*. 2019;14:2415–2431. doi:10.2147/IJN.S193676
31. Tzourio-Mazoyer N, Landeau B, Papathanassiou D, et al. Automated anatomical labeling of activations in SPM using a macroscopic anatomical parcellation of the MNI MRI single-subject brain. *Neuroimage*. 2002;15(1):273–289. doi:10.1006/nimg.2001.0978
32. Berlangieri A, Elliott S, Wasiak J, Chao M, Foroudi F. Use of magnetic resonance image-guided radiotherapy for breast cancer: a scoping review. *J Med Radiat Sci*. 2021. doi:10.1002/jmrs.545
33. Amirrashedi M, Alam NR, Mostaar A, Haghgoo S, Gorji E, Jaberi R Dose enhancement in radiotherapy by novel application of gadolinium based MRI contrast agent nanomagnetic particles in gel dosimetry. Paper presented at: World Congress on Medical Physics and Biomedical Engineering; Jun 07–12, 2015; Toronto, CANADA.
34. Seo SJ, Han SM, Cho JH, et al. Enhanced production of reactive oxygen species by gadolinium oxide nanoparticles under core-inner-shell excitation by proton or monochromatic X-ray irradiation: implication of the contribution from the interatomic de-excitation-mediated nanoradiator effect to dose enhancement. *Radiat Environ Biophys*. 2015;54(4):423–431. doi:10.1007/s00411-015-0612-7
35. Shen Z, Liu T, Yang Z, et al. Small-sized gadolinium oxide based nanoparticles for high-efficiency theranostics of orthotopic glioblastoma. *Biomaterials*. 2020;235:119783. doi:10.1016/j.biomaterials.2020.119783
36. Song H, Sun H, He N, et al. Gadolinium-based ultra-small nanoparticles augment radiotherapy-induced T-cell response to synergize with checkpoint blockade immunotherapy. *Nanoscale*. 2022;14(31):11429–11442. doi:10.1039/D2NR02620A
37. Zhang S, Wu Y, Yu J, et al. Gadolinium-bisphosphonate nanoparticle-based low-dose radioimmunotherapy for osteosarcoma. *ACS Biomater Sci Eng*. 2022;8(12):5329–5337. doi:10.1021/acsbiomaterials.2c00880
38. Böttcher JP, Bonavita E, Chakravarty P, et al. NK cells stimulate recruitment of cDC1 into the tumor microenvironment promoting cancer immune control. *Cell*. 2018;172(5). doi:10.1016/j.cell.2018.01.004
39. Deng L, Liang H, Xu M, et al. STING-dependent cytosolic DNA sensing promotes radiation-induced type I interferon-dependent antitumor immunity in immunogenic tumors. *Immunity*. 2014;41(5):843–852. doi:10.1016/j.immuni.2014.10.019
40. Rodríguez-Ruiz ME, Vanpouille-Box C, Melero I, Formenti SC, Demaria S. Immunological mechanisms responsible for radiation-induced abscopal effect. *Trends Immunol*. 2018;39(8):644–655. doi:10.1016/j.it.2018.06.001
41. Tomayko MM, Reynolds CP. Determination of subcutaneous tumor size in athymic (nude) mice. *Cancer Chemother Pharmacol*. 1989;24 (3):148–154. doi:10.1007/BF00300234
42. Munshi A, Hobbs M, Meyn RE. Clonogenic cell survival assay. *Chemosensitivity*. 2005;110:21–28.
43. Liu X, Li P, Hirayama R, et al. Genistein sensitizes glioblastoma cells to carbon ions via inhibiting DNA-PKcs phosphorylation and subsequently repressing NHEJ and delaying HR repair pathways. *Radiother Oncol*. 2018;129(1):84–94. doi:10.1016/j.radonc.2018.04.005
44. Liu X, Wang Q, Liu B, et al. Genistein inhibits radiation-induced invasion and migration of glioblastoma cells by blocking the DNA-PKcs/Akt2/Rac1 signaling pathway. *Radiother Oncol*. 2021;155:93–104. doi:10.1016/j.radonc.2020.10.026
45. Martina MS, Fortin JP, Menager C, et al. Generation of superparamagnetic liposomes revealed as highly efficient MRI contrast agents for in vivo imaging. *J Am Chem Soc*. 2005;127(30):10676–10685. doi:10.1021/ja0516460
46. Reppingen N, Helm A, Doleschal L, Durante M, Fournier C. A combination of cabozantinib and radiation does not lead to an improved growth control of tumors in a preclinical 4T1 breast cancer model. *Front Oncol*. 2021;11:788182. doi:10.3389/fonc.2021.788182
47. Hu H, Zheng S, Hou M, et al. Functionalized Au@Cu-Sb-S nanoparticles for spectral CT/photoacoustic imaging-guided synergetic photo-radiotherapy in breast cancer. *Int J Nanomed*. 2022;17:395–407. doi:10.2147/IJN.S338085
48. Liu X, Liu Y, Zhang P, et al. The synergistic radiosensitizing effect of tirapazamine-conjugated gold nanoparticles on human hepatoma HepG2 cells under X-ray irradiation. *Int J Nanomed*. 2016;11:3517–3531. doi:10.2147/IJN.S105348
49. Khoei S, Mahdavi SR, Fakhimikabir H, Shakeri-Zadeh A, Hashemian A. The role of iron oxide nanoparticles in the radiosensitization of human prostate carcinoma cell line DU145 at megavoltage radiation energies. *Int J Radiat Biol*. 2014;90(5):351–356. doi:10.3109/09553002.2014.888104
50. Huang F-K, Chen W-C, Lai S-F, et al. Enhancement of irradiation effects on cancer cells by cross-linked dextran-coated iron oxide (CLIO) nanoparticles. *Phys Med Biol*. 2010;55(2):469–482. doi:10.1088/0031-9155/55/2/009
51. Ding Y, Xiao X, Zeng L, et al. Platinum-crosslinking polymeric nanoparticle for synergetic chemoradiotherapy of nasopharyngeal carcinoma. *Bioact Mater*. 2021;6(12):4707–4716. doi:10.1016/j.bioactmat.2021.05.010

52. Caro C, Carmen Munoz-Hernandez M, Leal MP, Garcia-Martin ML. In vivo pharmacokinetics of magnetic nanoparticles. *Methods Mol Biol*. 2018;1718:409–419.
53. Detappe A, Mathieu C, Jin C, et al. Anti-MUC1-C antibody-conjugated nanoparticles potentiate the efficacy of fractionated radiation therapy. *Int J Radiat Oncol Biol Phys*. 2020;108(5):1380–1389. doi:10.1016/j.ijrobp.2020.06.069
54. Samson N, Ablasser A. The cGAS-STING pathway and cancer. *Nat Cancer*. 2022;3(12):1452–1463. doi:10.1038/s43018-022-00468-w
55. Sun LJ, Wu JX, Du FH, Chen X, Chen ZJJ. Cyclic GMP-AMP synthase is a cytosolic DNA sensor that activates the type I interferon pathway. *Science*. 2013;339(6121):786–791. doi:10.1126/science.1232458